PASJ: Publ. Astron. Soc. Japan **65**, 24, 2013 April 25

The GENJI Programme: Gamma-Ray Emitting Notable AGN Monitoring by Japanese VLBI

Hiroshi NAGAI,[1] Motoki KINO,[1] Kotaro NIINUMA,[2] Kazunori AKIYAMA,[3,1,*] Kazuhiro HADA,[4] Shoko KOYAMA,[3,1] Monica ORIENTI,[4,5] Koichiro HIURA,[6] Satoko SAWADA-SATOH,[7] Mareki HONMA,[1] Gabriele GIOVANNINI,[4,5] Marcello GIROLETTI,[4] Katsunori SHIBATA,[1] and Kazuo SORAI [6]

[1]*National Astronomical Observatory of Japan, 2-21-1 Osawa, Mitaka, Tokyo 181-8588*
hiroshi.nagai@nao.ac.jp
[2]*Graduate School of Science and Engineering, Yamaguchi University, 1677-1 Yoshida, Yamaguchi, Yamaguchi 753-8512*
[3]*Department of Astronomy, Graduate School of Science, The University of Tokyo, 7-3-1 Hongo, Bunkyo-ku, Tokyo 113-0033*
[4]*INAF Istituto di Radioastronomia, via Gobetti 101, 40129 Bologna, Italy*
[5]*Dipartimento di Astronomia, Università di Bologna, via Ranzani 1, I-40127 Bologna, Italy*
[6]*Department of Cosmosciences, Graduate School of Science, Hokkaido University, Kita 10, Nishi 8, Kita-ku, Sapporo 060-0810*
[7]*Mizusawa VLBI Observatory, National Astronomical Observatory of Japan, 2-12 Hoshigaoka-cho, Mizusawa-ku, Oshu, Iwate 023-0861*

(Received 2012 September 7; accepted 2012 October 8)

Abstract

We introduce the gamma-ray emitting notable active galactic nucleus (AGN) monitoring by Japanese VLBI programme, which is the monitoring of gamma-ray bright AGNs with the VLBI Exploration of Radio Astrometry (VERA) array. This programme aims to conduct dense monitoring at 22 GHz toward the γ-ray emitting AGNs to investigate the time variation of the radio core and possible ejection of a new radio component, the motion of jets, and their relations with the emission at other wavelengths, especially at γ-rays. We are currently monitoring 8 notable γ-ray-emitting AGNs (DA 55, 3C 84, M 87, PKS 1510−089, DA 406, NRAO 530, BL Lac, and 3C 454.3) about once every two weeks. This programme is promising for tracing the trend of radio time variation on shorter time scale than conventional VLBI monitoring programmes and is complementary to data of other programmes (e.g., MOJAVE; Boston University Blazar Project). In particular, we successfully carried out quick follow-up observations after the GeV γ-ray flare in NRAO 530 and 3C 454.3 reported by the Fermi Gamma-ray Space Telescope. Here, we present the initial results of morphology and light curves for the first 7-month operation.

Key words: galaxies: active — galaxies: individual (DA 55, 3C 84, M 87, PKS 1510−089, DA 406, NRAO 530, BL Lacertae, 3C 454.3) — galaxies: jets — radio continuum: galaxies

1. Introduction

Nonthermal emission from relativistic jets emanating from supermassive black holes usually dominates in the wide range of electromagnetic spectrum from radio to γ-rays. Some emissions appear up in a very high energy range, even in the GeV and TeV γ-ray energy ranges. The location of high-energy emission and its production mechanism are long-standing problem in active galactic nucleus (AGN) jet physics. With the recent progress of the Large Area Telescope (LAT) onboard Fermi Gamma-ray Space Telescope and new generation Cherenkov telescopes, such as H.E.S.S., MAGIC, and VERITAS, we have a new opportunity to explore jet physics in connection with γ-ray emission. The number of AGN-hosted γ-ray sources has drastically increased compared to that in the era of the Energetic Gamma-ray Experiment Telescope (EGRET)/CGRO (Nolan et al. 2012), including new discoveries of γ-ray emission from misaligned AGNs (e.g., Abdo et al. 2010a). While a number of competing models have been proposed (e.g., Sikora et al. 2009 and references therein), the γ-ray emission mechanism and the location of the emitting region are still disputed. Quasi-simultaneous multiwavelength studies are the key to discrimination between such models.

At radio wavelengths, the high angular resolution provided by Very Long Baseline Interferometry (VLBI) is essential to identifying the radio counterpart of the γ-ray emitting site in AGN jets. In the conventional framework of spectral energy distribution (SED) modeling with the one-zone synchrotron-self Compton model and/or external Compton, the blazars should have a subparsec-sized emission region, or an even smaller size (Kubo et al. 1998), and the emission region is possibly associated with the region close to the jet base. Ultimately, VLBI has a potential for identifying the exact location of the γ-ray emitting region. In addition, VLBI is a unique tool for measuring the jet motion, which allows us to investigate whether the γ-rays beamed with the same Lorentz factor as indicated by the VLBI motion.

The γ-ray luminosity shows a definite correlation with the radio luminosity over more than 4 orders of magnitude (Lister et al. 2011). This seems to indicate a tight connection between the γ-ray and radio properties in AGN jets. So far, considerable effort has been expended to do intensive VLBI monitoring

* Research Fellow of Japan Society for the Promotion of Science (JSPS).

Table 1. Sources.

Source	Alias	z	pc/mas*	Optical ID†
J0136+4751	DA 55	0.859	7.759	FSRQ
J0319+4130	3C 84	0.0176	0.344	NLRG/Sy2
J1230+1223	M 87	0.004360	0.112	NLRG
J1512−0905	PKS 1510−089	0.36	5.043	Sy1/HPQ
J1613+3412	DA 406	1.39712	8.568	FSRQ
J1733−1304	NRAO 530	0.902	7.879	FSRQ/LPQ
J2202+4216	BL Lac	0.0686	1.289	BLLAC
J2253+1608	3C 454.3	0.859	7.757	FSRQ/HPQ

* Linear size of 1 mas.
† FSRQ, flat spectrum radio quasars; NLRG, narrow line radio galaxies; Sy1, Seyfert type-1; Sy2, Seyfert type-2; HPQ, highly polarized quasars; LPQ, low polarized quasars; BLLAC, BL Lac objects.

in the context of the radio–γ-ray connection. However, not all of the γ-ray events in blazars and radio galaxies have a clear radio counterpart, as in the case of the GeV–TeV γ-ray flare in 3C 279 (Abdo et al. 2010b) and the GeV γ-ray flare in 3C 84 (Nagai et al. 2012). Another intriguing case in PKS 1510−089 is that some γ-ray flares seem to be related to the change in the radio band (e.g., Marscher et al. 2010; Orienti et al. 2011), while the others have no relation to it (e.g., D'Ammando et al. 2009). Therefore, the location of the radio counterpart of the γ-ray emission is still an open question, and additional validations in more samples are highly awaited.

The Gamma-ray Emitting Notable AGN Monitoring by Japanese VLBI (GENJI) programme aims at dense monitoring of γ-ray bright AGNs using VLBI Exploration Radio Astrometry (VERA). VERA aims at Galactic maser astrometry, but for technical reasons it needs to observe a bright calibrator once every $\sim$80 min. We use this calibrator time as the slot for GENJI sources. Since most of VERA projects are carried out at 22 GHz, the frequency of the GENJI observation is also basically limited to 22 GHz. However, sometimes we can perform a 43 GHz observation, depending on the aim of the VERA project (e.g., SiO maser observation).[1] The goal of the GENJI programme is to study the correlation in the time variability between γ-ray and radio components, including the radio core and some other jet components, in order to identify a possible radio counterpart of the γ-ray emission. We also aim to measure the apparent motion of the jet, thus allowing us to calculate the jet speed. We focus on the time variation on a time scale of shorter than 1 month, and a quick follow-up observation after the γ-ray flare. Currently, we are carrying out this monitoring once every two weeks. Such dense monitoring is unique at 22 GHz in the northern hemisphere (cf. TANAMI in the southern hemisphere: Ojha et al. 2010). We can thus obtain complementary data with the other monitoring projects (e.g., MOJAVE,[2] Lister et al. 2009; Boston University Blazar Projects[3]).

The GENJI observation started in 2010 November. We have already detected radio flaring associated with a GeV flare in PKS 1510−089 (Orienti et al. 2012). In addition, we successfully coordinated observations just before and after the GeV flare in 3C 454.3 and NRAO 530; the results are now in preparation. In this paper, we present the quality of the data and the initial results for the first 7-month data. Throughout the paper we adopt the following cosmological parameters: $H_0 = 70.2\,\mathrm{km\,s^{-1}\,Mpc^{-1}}$, $\Omega_\mathrm{M} = 0.27$, and $\Omega_\Lambda = 0.73$ (Komatsu et al. 2011).

2. Sample

We do not demand statistical completeness of AGN jets, but rather aim at dense sampling for particular sources. The GENJI sample consists of seven bright blazars and two radio galaxies (3C 84 and M 87). The sample was selected from the VLBA 2 cm survey (Kellermann et al. 1998) and the monitoring of jets in active galactic nuclei with VLBA experiments (MOJAVE) programme (Lister et al. 2009), whose expected, correlated flux density is brighter than $\sim$1 Jy to fulfill the role of fringe finder or delay calibrator for the VERA project observation, identified as a GeV γ-ray source by Fermi/LAT. Because GENJI observations should be carried out within short-time slots so as not to disrupt the total observing time for the VERA project by antenna slewing as quickly as possible, we can basically choose sources close to the target source of the VERA project on the celestial plane. We finally selected 8 sources, listed in table 1. Plots of typical interferometric *uv*-coverage are shown in figure 1. OJ 287 has been included in the GENJI sample since 2011 December.

3. Observation and Data Reduction

Observations were carried out using the VERA 4 stations. Monitoring was suspended from 2011 March 11 to 2011 April 19 because of a big earthquake shaking the northeast of Japan. During the period from 2011 June to 2011 August, the VERA was not able to be used because of maintenance. Most of the sources were observed at 22 GHz. Sometimes 43 GHz observations were also performed, but we do not include the results in this paper. The on-source time for each observation was typically 30 minutes, spreading over 4–6 scans at different hour angles. Each source of the sample was observed almost

[1] Since VERA has no frequency agility, we cannot conduct both 22 and 43 GHz observations at the same time.
[2] ⟨http://www.physics.purdue.edu/MOJAVE/index.html⟩.
[3] ⟨http://www.bu.edu/blazars/research.html⟩.

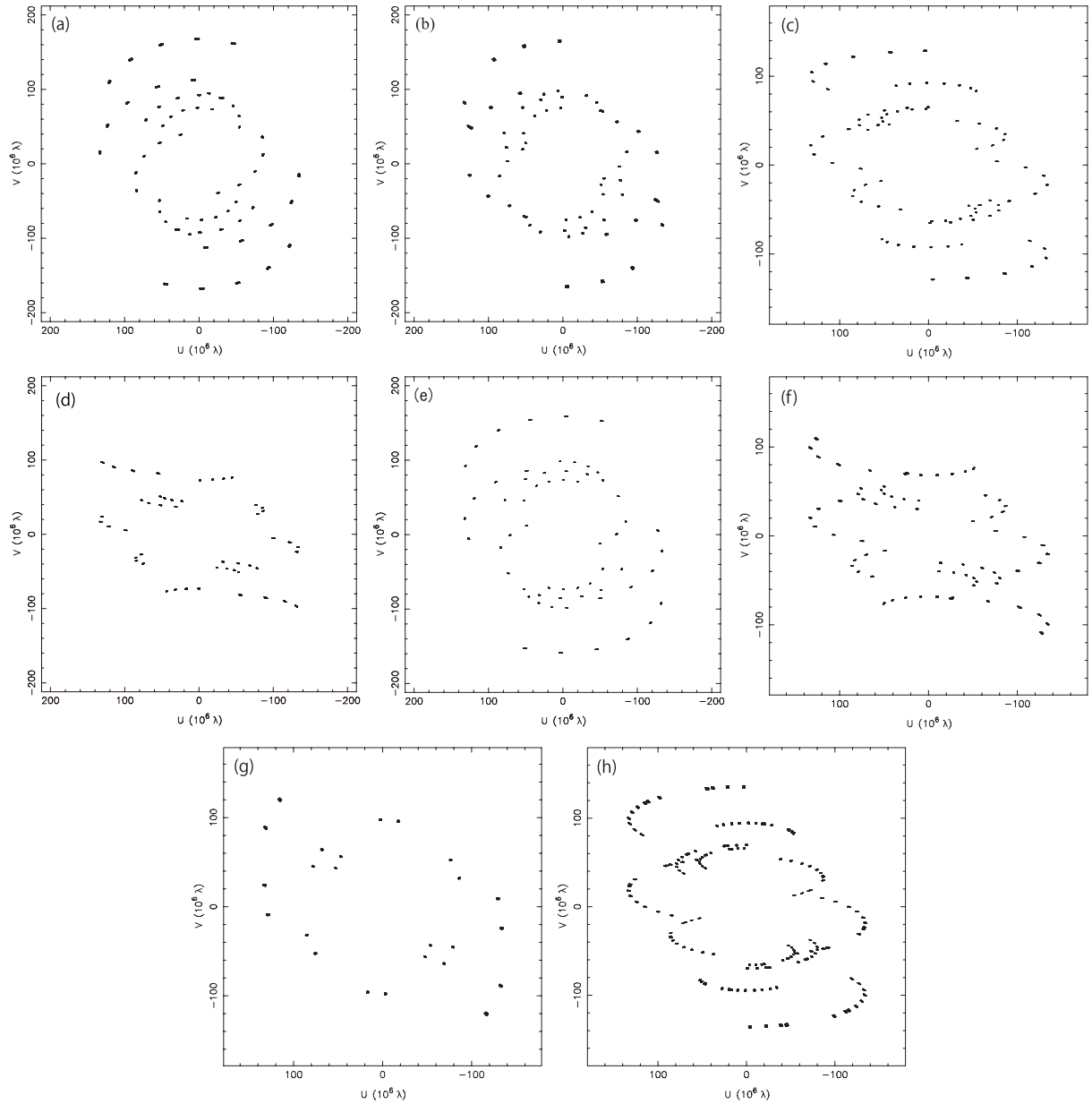

Fig. 1. Examples of *uv*-coverage. (a) DA 55, (b) 3C 84, (c) M 87, (d) PKS 1510−089, (e) DA 406, (f) NRAO 530, (g) BL Lac, and (h) 3C 454.3.

once every two weeks.

Left-hand circular polarization signals were received and sampled with 2-bit quantization, and filtered using the VERA digital filter unit (Iguchi et al. 2005). The data were recorded at a rate of 1024 Mbps. The baseband allocation depended on the observation, but mostly providing a band-width of 256 MHz, in which 14 IF-channels per a total of 15 IF-channels of 16 MHz bandwidth were assigned to the GENJI source. Because of significant signal loss ($\sim$30%), due to an analog filter implemented in front of the digital filter, we did not use the data of the 12th, 13th, and 14th IFs. Correlation processes were undergone on the Mitaka FX correlator (Chikada et al. 1991).

Data reduction was performed using the NRAO Astronomical Image Processing System (AIPS). As a first step in the data reduction, we flagged the data of 10 channels at both edges of the band in each IF, and then normalized the cross-correlation by autocorrelation. A standard *a priori* amplitude calibration was performed using the AIPS task APCAL, based on measurements of the system temperature ($T_{\rm sys}$) by the chopper-wheel method during the observation, and the aperture efficiency provided in the VERA Status Report in 2009. We did not employ the opacity correction in the task APCAL, since the $T_{\rm sys}$ derived from the chopper-wheel method includes the effect of atmospheric absorption. This amplitude calibration provides an accuracy of $\sim$10%, according to a number of experiences involving VERA observations (e.g., Petrov et al. 2012). Fringe fitting was done using the AIPS task FRING. After carefully flagging the bad data

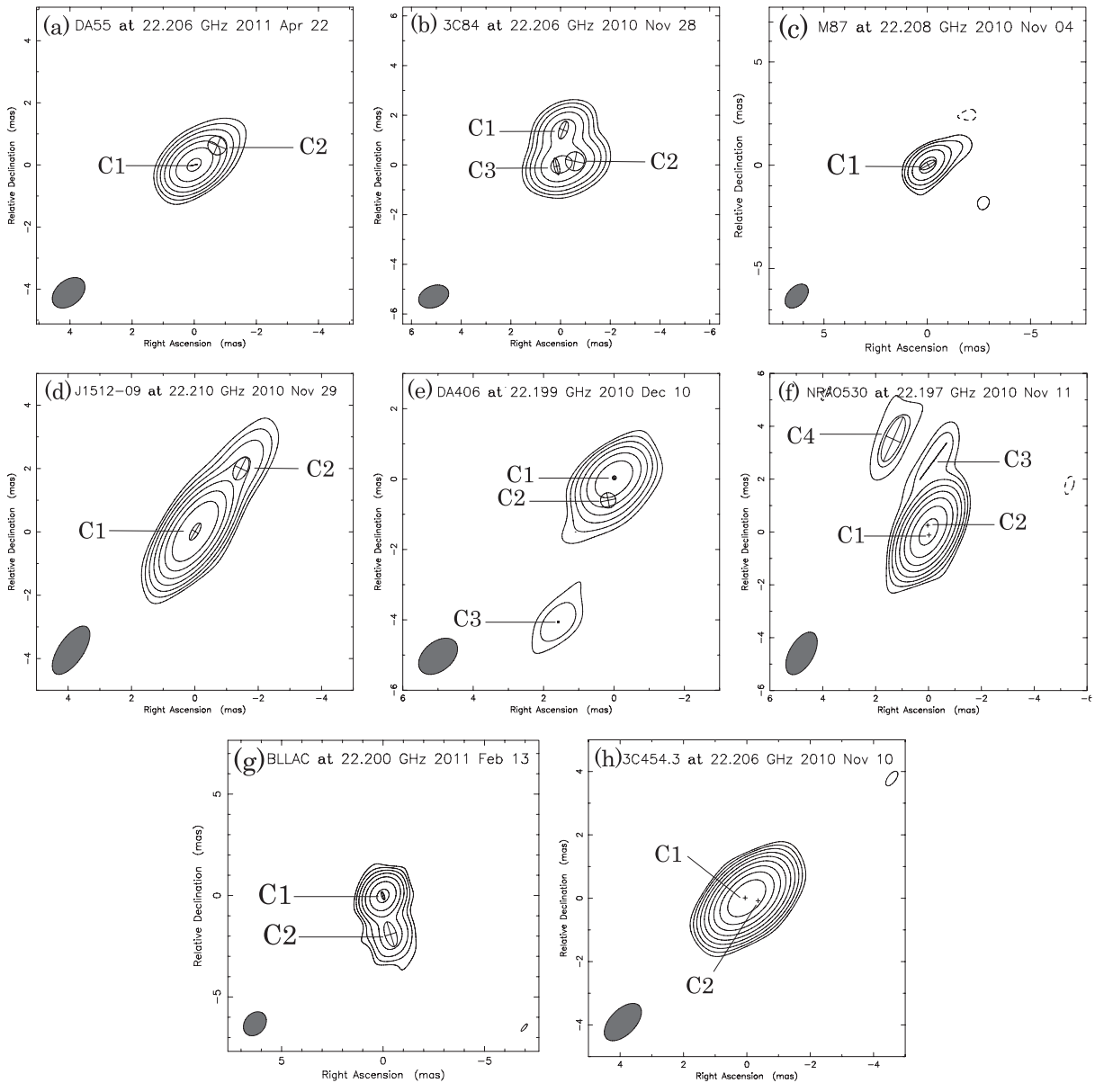

Fig. 2. Examples of a Gaussian model fit. (a) DA 55, (b) 3C 84, (c) M 87, (d) PKS 1510−089, (e) DA 406, (f) NRAO 530, (g) BL Lac, and (h) 3C 454.3. The total intensity image is created by CLEAN, and a model-fit image is produced by restoring the model-fit components.

and averaging 10 s in the time domain and over a bandpass, we constructed the initial source model using the CLEAN algorithm implemented in the Difmap software package, and performed self-calibration adjusting the visibility phase so as to minimize the residual error with conserving the closure phase. We performed a number of iterations with CLEAN as well as phase self-calibration. When the residual error between the model and observed visibility converged, then we switched to both phase and amplitude self-calibration if they work.

For some observations, we combined multiple *uv*-data sets taken within a few days so as to improve the *uv*-coverage. This was done by the AIPS task DBCON after *a priori* amplitude and phase calibrations. After combining the data sets, we performed imaging, as described above.

3.1. Modeling the Data

To quantify the position, size, and flux density of the core and jet components, we modeled the source by multiple Gaussian components. We fitted elliptical Gaussians to the visibility data using the *modelfit* task in Difmap. The goodness of the fit was judged by relative χ^2 statistics. We sometimes used elliptical Gaussians or point sources if they could produce better fits and consistency across the epochs. Figure 2 shows examples of model-fit images. Note that these images are essentially similar to the total intensity images produced by CLEAN (figures 3–10), thus demonstrating the validity of the modeling procedure.

4. Flux Density and Positional Accuracy

It is important to check the flux density and the positional accuracy when studying the time variation. Among eight sources, we obtained a subset of two or three images observed within a very short time scale ($\sim$ a week) for 3C 84, NRAO 530, 3C 454.3, and BL Lac. Using these four sources, we checked the consistency of the flux density of each component. In table 2 we give the calculated $\Delta S = \sigma/\bar{S}$ for each source, where σ is the standard deviation of the flux density among epochs, and $\bar{S}$ is the flux density averaged over the epochs given in tables 3–10. The resultant ΔS for the core component was less than 7.5%, which did not exceed the typical flux calibration error of VERA, $\sim 10\%$ (see section 3). On the other hand, ΔS values of the other jet components were typically 20%, probably because of a lack of sampling on the *uv*-plane. Thus, we adopted 10% for the flux error of the core component and 20% for that of other jet components. One exception was that all three components (C1, C2, and C3) of 3C 84 are in good agreement concerning the flux density among three epochs ($\Delta S \lesssim 6\%$). We adopted a flux error of 10% for all components of 3C 84.

We also checked the consistency of the component position with reference to the core, and found that the difference in position between epochs was typically ~ 0.1 mas. However, the result of the position for component C2 of PKS 1510−089 was quite variable. This is probably due to the existence of multiple subcomponents in C2 (see subsection 7.4). In this paper, we assume that the typical positional accuracy is ~ 0.1 mas, but more details will be elaborated in a forthcoming paper.

5. Results

5.1. Images

In figures 3–10, we show three images in adjacent observing epochs for each source. We convolved each image with an identical beam, which was the largest beam among three epochs for each source. For each image, we provide the beam size, contour levels, and peak intensity in the caption. Image noises were generally between 10 and 30 mJy beam^{-1}. The noise of 3C 454.3 image was 76 mJy beam^{-1}, since the dynamic range of image was limited by the very bright (more than 20 Jy) core. The physical parameters of Gaussian models for these three epochs are summarized in tables 3–10. All sources exhibited a bright core and a few additional components in the jet. Because of a lack of short base lines, we only detected the structure within ~ 3 mas from the core, but missed extended structures.

5.2. Light Curves

In figure 11, we plot the light curve of our GENJI programme during the first 7 months, and the MOJAVE light curve during the same period. For the GENJI data, we plot the light curve of each component described in subsection 3.1 in addition to that of the total flux density. For the MOJAVE data, we plot the light curve of the total flux density. The flux error due to the model-fit error is negligible, as compared to the flux calibration error. We assumed that the flux error of MOJAVE is 5%. It is obvious from figure 11 that the sampling interval of GENJI during this period is much shorter than that of MOJAVE.

6. Consistency Check on Flux Density with MOJAVE

In this section, we compare the light curve of GENJI with that of MOJAVE. MOJAVE provides the flux density once every two or three months; the observing frequency, 15 GHz, is nearly the same as the GENJI observing frequency, 22 GHz. Therefore, the MOJAVE data can be a check on the fidelity of the GENJI data.

In particular for PKS 1510−089, there are two MOJAVE data that were observed in nearly the same epochs as the GENJI data. The flux densities from GENJI were 1.92 Jy on 2010 November 29 and 2.31 Jy on 2011 February 26, while those from MOJAVE were 1.69 Jy on 2010 November 29 and 2.16 Jy on 2011 February 27. The flux densities of GENJI were 10%–20% higher than those of MOJAVE in both epochs. Since most of the flux density originates in the core, and the core has a slightly inverted spectrum with a spectral index (α) of 0.2 (Sokolovsky et al. 2010), these differences in the flux density between GENJI and MOJAVE are reasonable.

Another good example is BL Lac. Although we do not have good overlaps in the observing period between MOJAVE and GENJI, two trends of the light curve during the 7 months are very similar. The GENJI flux density is always smaller than the MOJAVE flux density by ~ 1 Jy, but this difference can be explained by the contribution from the extended jet. A continuous jet extending up to more than 5 mas from the core is seen on the MOJAVE images (Lister et al. 2009). This extending jet cannot be time variable, as compared to the core. Therefore, the similarity in the light curve between GENJI and MOJAVE demonstrates the repeatability of the flux

Table 2. Flux error estimation.

Source	Components	ΔS^*
3C 84[†]	C1	0.011
	C2	0.062
	C3	0.057
PKS 1510−089[‡]	C1	0.018
	C2	0.215
NRAO 530[§]	C1+C2	0.012
	C3	0.208
BL Lac[#]	C1	0.075
	C2	0.18
3C 454.3[**]	C1+C2	0.031

* $\Delta S = \sigma/\bar{S}$, where σ is the standard deviation of the flux density among observation epochs and $\bar{S}$ is the flux density averaged over the epochs.

† ΔS is calculated from the data on 2010/Nov/28, 2010/Nov/29, and 2010/Dec/04.

‡ ΔS is calculated from the data on 2010/Nov/29 and 2010/Dec/04.

§ ΔS is calculated from the data on 2010/Nov/11, 2010/Nov/14 and 2010/Nov/16.

ΔS is calculated from the data on 2011/Feb/8, 2011/Feb/12, and 2011/Feb/13.

** ΔS is calculated from the data on 2010/Nov/10 and 2010/Nov/12.

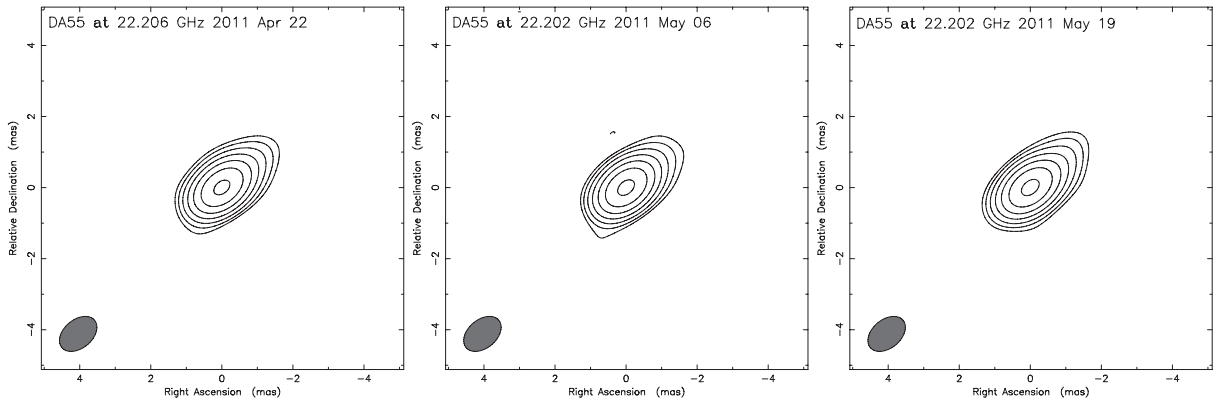

Fig. 3. Total intensity images of DA 55. All images are convolved by an identical synthesized beam of (1.2×0.8) mas at a position angle of $-50°$. The contours are plotted at the level of $0.025 \times (-1, 1, 2, 4, 8, 16, 32, 64)$ Jy beam^{-1}. The peak intensities of three images (left, middle, and right panels) are 1.80, 1.83, and 1.84 Jy beam^{-1}, respectively.

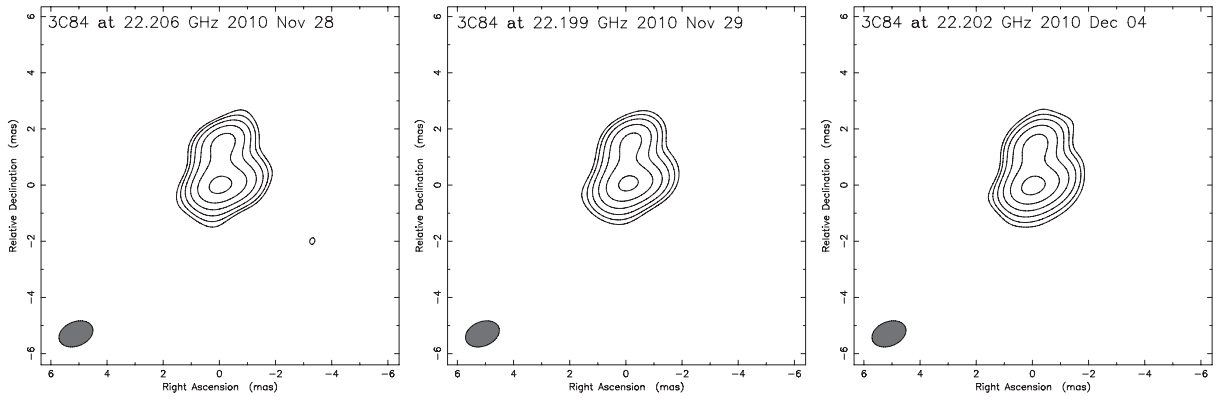

Fig. 4. Total intensity images of 3C 84. All images are convolved by an identical synthesized beam of (1.26×0.861) mas at a position angle of $-67.^{\circ}4$. The contours are plotted at the level of $18.1 \times (-1, 1, 2, 4, 8, 16, 32)$ mJy beam^{-1}. The peak intensities of three images (left, middle, and right panels) are 7.05, 6.79, and 7.27 Jy beam^{-1}, respectively.

measurement by GENJI.

Although there are not so many overlaps, a similar trend in the light curve is apparent in NRAO 530 and 3C 454.3.

In summary, our GENJI programme is promising for providing dense monitoring data for the flux measurement.

7. Notes on Individual Sources

In this section we describe the morphology and light curve for each source after a brief review of the background information and previous observations.

7.1. J0136+4751 (DA 55)

DA 55 is classified as a Flat Spectrum Radio Quasar (FSRQ) at $z = 0.859$ (Healey et al. 2008). This source is listed in the Fermi/LAT bright γ-ray source (0FGL J0137.1+4751), though it was not detected by EGRET. The γ-ray flux density of DA 55 in 2009 mid-March reached about three times the averaged flux density in the first-year light curve (Abdo et al. 2010c). The parsec-scale jet feature is one-sided in the VLBA 15 GHz total intensity image (Lister et al. 2009). The jet moves toward the north-west.

We detected the jet feature in the position angle of $\sim -45°$ within ~ 2 mas from the core (C1) (figures 2a and 3). A single Gaussian component, C2, can be fitted to this jet. Until 2010, a bright jet component (a few hundred of mJy), located at ~ 4 mas from the core in the position angle $\sim -40°$, can be seen in the MOJAVE images. This outer component has not been visible in both the GENJI and MOJAVE images because of its faintness, since the GENJI programme started.

We have not obtained much data for this source so far. No significant change in the flux density has been detected.

7.2. J0319+4130 (3C 84)

The bright radio source 3C 84 ($z = 0.0176$: Petrosian et al. 2007) shows two-sided radio jets/lobes on the north and the south of the core in the central 5 pc (Walker et al. 2000; Asada et al. 2006). In the mid-1980s, the radio-flux density became exceptionally bright, more than 60 Jy at centimeter wavelengths (e.g., O'Dea et al. 1984), and then subsequently decreased, such that until the early 2000s the radio-flux density decreased to ~ 10 Jy. The radio-flux density has started to increase since 2005 (Abdo et al. 2009a). This source came to be known as a γ-ray source after four months of operation of Fermi (Abdo et al. 2009a); 3C 84 is a typical example of sources exhibiting a clear time variation in the GeV

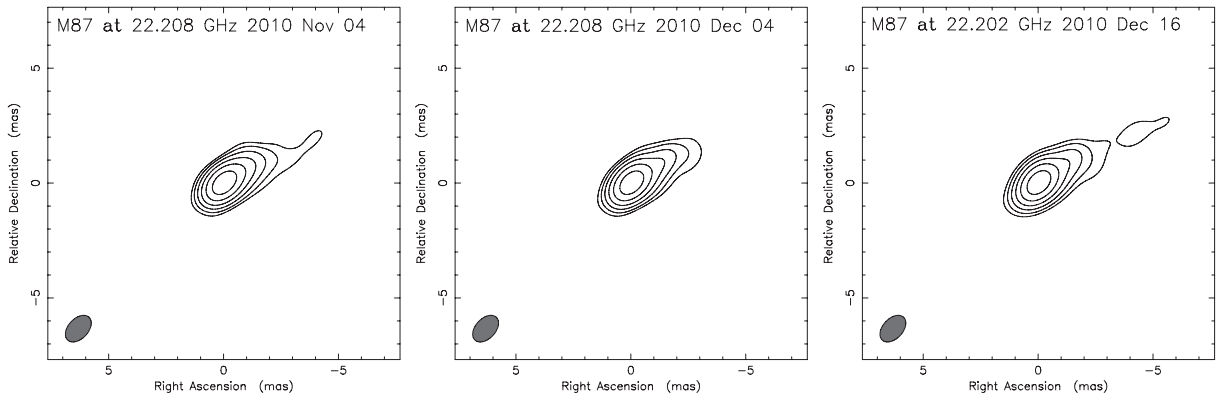

Fig. 5. Total intensity images of M 87. All images are convolved by an identical synthesized beam of (1.36 × 0.87) mas at a position angle of −43°. The contours are plotted at the level of 18 × (−1, 1, 2, 4, 8, 16, 32) mJy beam^{-1}. The peak intensities of three images (left, middle, and right panels) are 0.95, 0.95, and 0.95 Jy beam^{-1}, respectively.

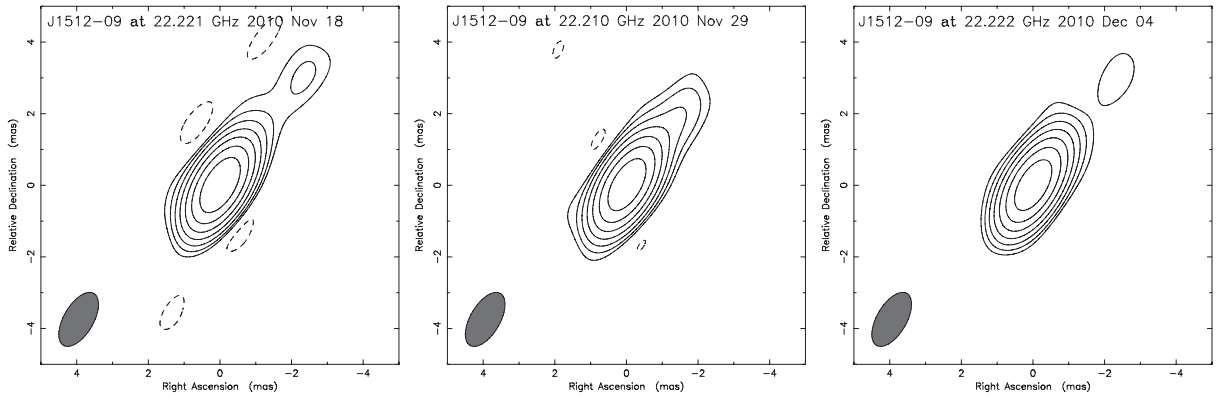

Fig. 6. Total intensity images of PKS 1510−089. All images are convolved by an identical synthesized beam of (1.68 × 0.828) mas at a position angle of −30.°3. The contours are plotted at the level of 14 × (−1, 1, 2, 4, 8, 16, 32, 64) mJy beam^{-1}. The peak intensities of three images (left, middle, and right panels) are 1.82, 1.66, and 1.62 Jy beam^{-1}, respectively.

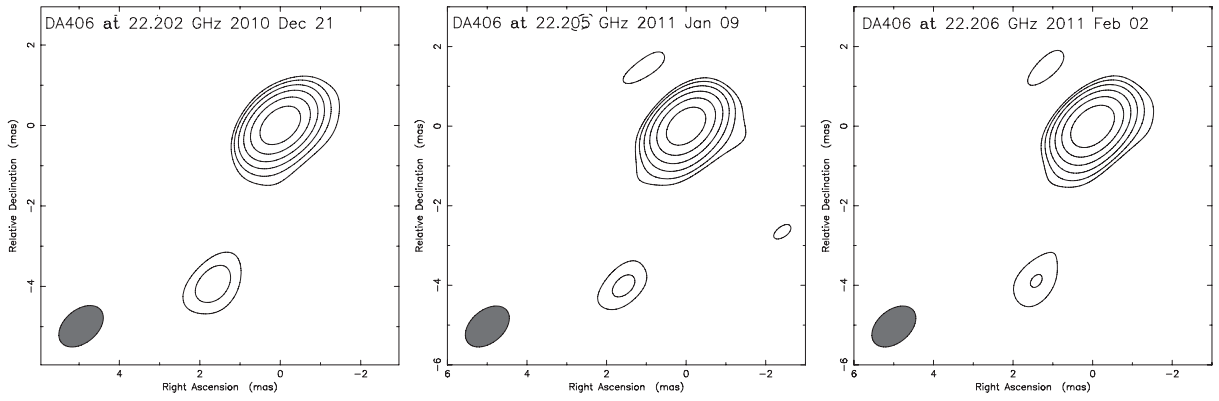

Fig. 7. Total intensity images of DA 406. All images are convolved by an identical synthesized beam of (1.27 × 0.82) mas at a position angle of −50°. The contours are plotted at the level of 22 × (−1, 1, 2, 4, 8, 16, 32) mJy beam^{-1}. The peak intensities of three images (left, middle, and right panels) are 1.26, 1.17, and 1.27 Jy beam^{-1}, respectively.

band among the misaligned γ-ray AGNs (Kataoka et al. 2010; Brown & Adams 2011). The MAGIC Cherenkov telescope also deteced very high-energy γ-ray emission with a spectral cut-off at around 100 GeV (Aleksić et al. 2012).

The central 1 pc structure consists of three components: C1, C2, and C3 (figure 2b). Images at the same frequency with similar resolution in earlier epochs were presented by Nagai et al. (2010). In figure 4, emission slightly extending from C3 to the south can be seen. This extending emission was increasingly visible in later epochs. An additional minor component

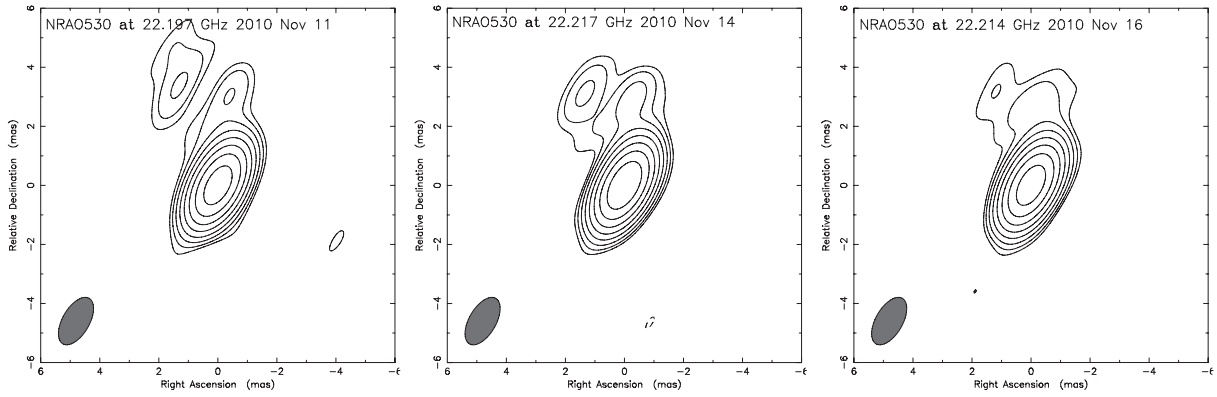

Fig. 8. Total intensity images of NRAO 530. All images are convolved by an identical synthesized beam of (1.78 × 0.911) mas at a position angle of −30°. The contours are plotted at the level of 22 × (−1, 1, 2, 4, 8, 16, 32, 64, 128) mJy beam^{-1}. The peak intensities of three images (left, middle, and right panels) are 3.94, 3.98, and 3.89 Jy beam^{-1}, respectively.

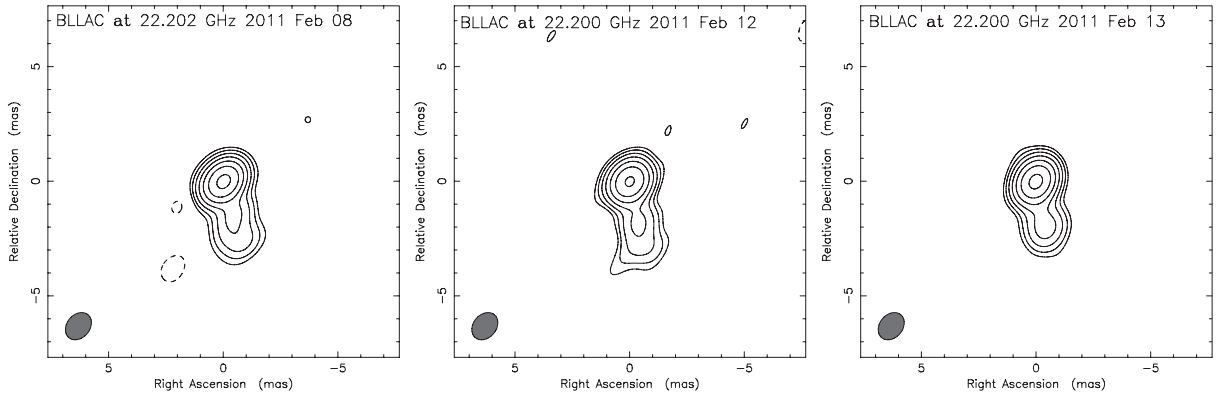

Fig. 9. Total intensity images of BL Lac. All images are convolved by an identical synthesized beam of (1.3 × 1.0) mas at a position angle of −40°. The contours are plotted at the level of 30 × (−1, 1, 2, 4, 8, 16, 32, 64) mJy beam^{-1}. The peak intensities of three images (left, middle, and right panels) are 2.30, 2.08, and 2.30 Jy beam^{-1}, respectively.

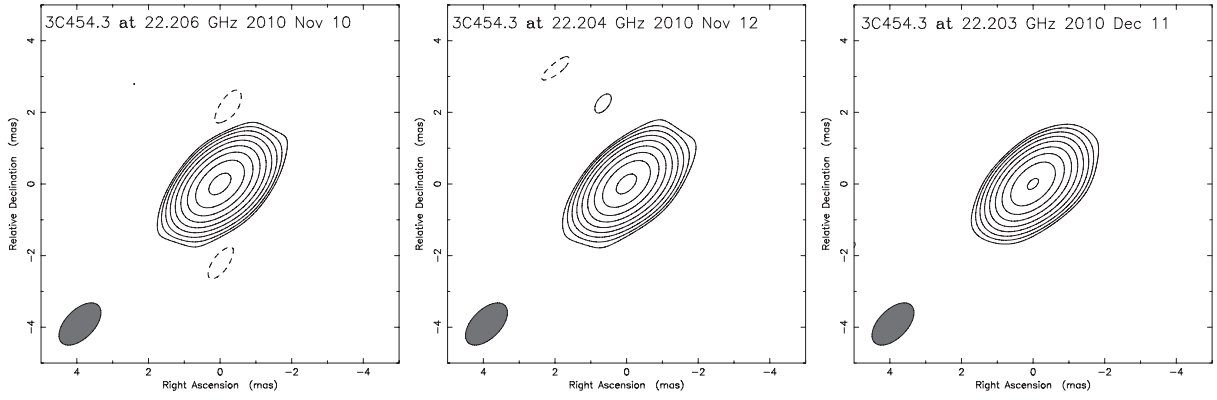

Fig. 10. Total intensity images of 3C 454.3. All images are convolved by an identical synthesized beam of (1.46 × 0.797) mas at a position angle of −44.°7. The contours are plotted at the level of 76.3 × (−1, 1, 2, 4, 8, 16, 32, 64, 128, 256) mJy beam^{-1}. The peak intensities of three images (left, middle, and right panels) are 23.5, 22.7, and 23.4 Jy beam^{-1}, respectively.

can be fitted to a structure located at ∼2 mas south from C3 in a few latest epochs after 2011 April (figure 12).

While there are only two data by MOJAVE, GENJI provides a light curve in more detail (figure 11b). The difference in the flux density between MOJAVE and GENJI is a few Jy, but it can be explained by the contribution from the extended jet that is not recovered by VERA observations, since more extended emission is detected in MOJAVE images (Lister et al. 2009). While the flux density increased steadily at 22 GHz and 43 GHz before 2009 (Nagai et al. 2010; Suzuki et al. 2012), the light

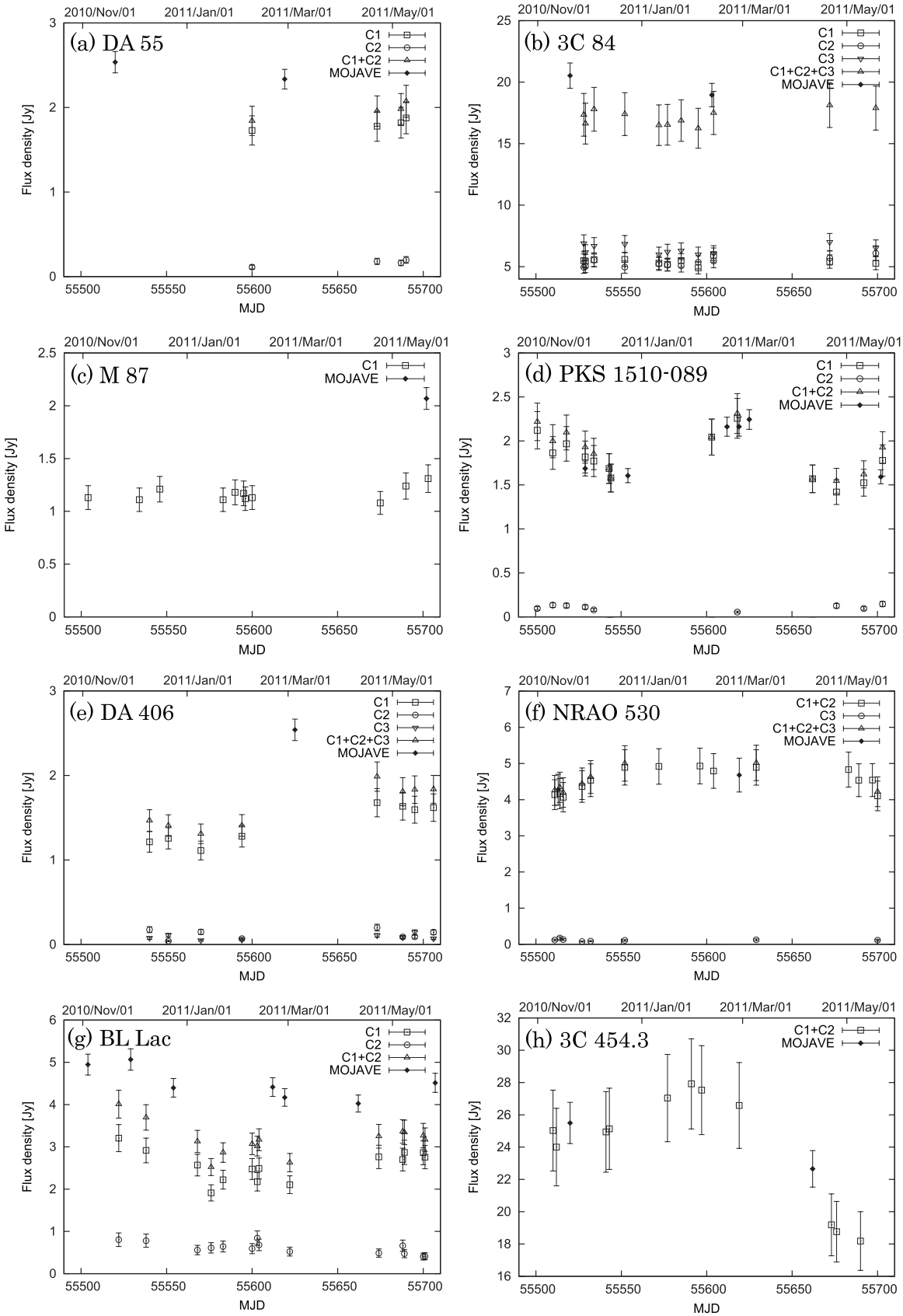

Fig. 11. First 6-month light curve of (a) DA 55, (b) 3C 84, (c) M 87, (d) PKS 1510−089, (e) DA 406, (f) NRAO 530, (g) BL Lac, and (h) 3C 454.3. For comparison, MOJAVE flux data are also plotted.

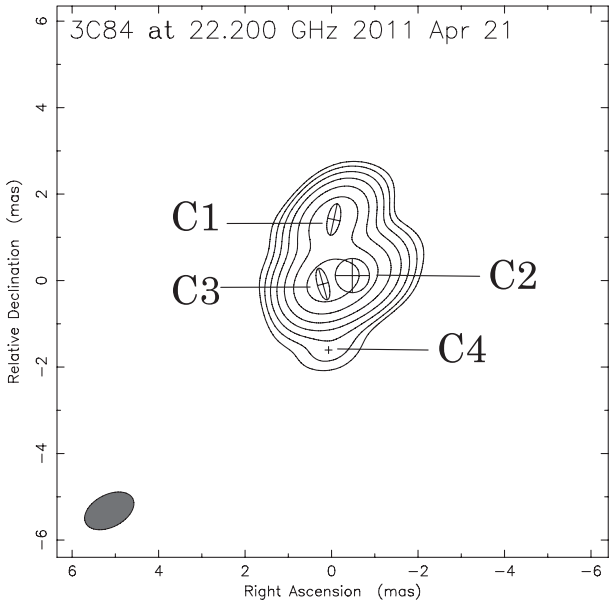

Fig. 12. Model-fit image of 3C 84 on 2011 April 21. A point source, C4, can be fitted ~ 2 mas south of C3.

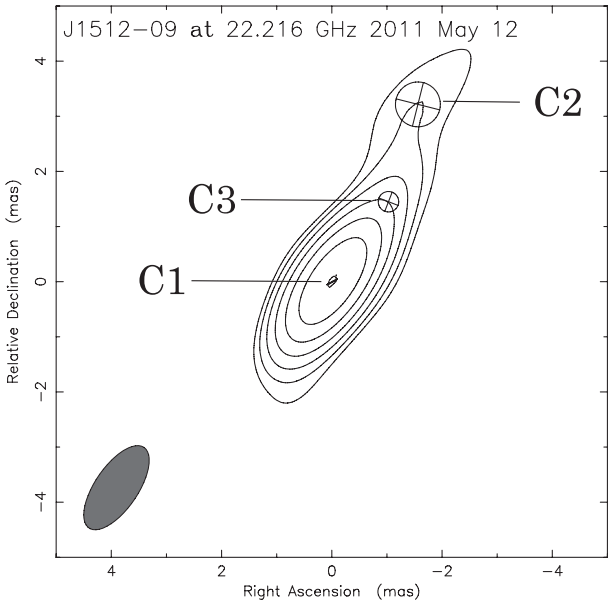

Fig. 13. Model-fit image of PKS 1510−089 on 2011 May 12.

curve presented here does not show any flux-density change within a level of 10%. Light curves at 37 GHz in the same periods are presented in Nagai et al. (2012), and besides, the 37 GHz flux density does not change very much.

7.3. J1230+1223 (M 87)

M 87 is a giant radio galaxy at the center of the Virgo cluster with a well-known one-sided jet. Its proximity ($z = 0.00436$: Rines & Geller 2008) provides a linear resolution of 1 mas $= 0.08$ pc, corresponding to $\sim 140\,R_{\rm s}$ for the mass of the central black hole, $M_{\rm BH} \sim 6 \times 10^9\,M_\odot$ (Gebhardt & Thomas 2009). This source has been routinely detected at energies of MeV/GeV (Abdo et al. 2009c) and TeV (e.g., Aharonian et al. 2006; Acciari et al. 2009; Abramowski et al. 2012). During the flaring activity at TeV in 2008, simultaneous VLBI observations detected a large increase of the flux density from the radio core (Acciari et al. 2009), whose location is specified as $\sim 20\,R_{\rm s}$ from the black hole (Hada et al. 2011). On the other hand, a distinct multiwavelength correlation was found for the recent TeV flaring event in 2010 April, where the core was relatively stable in radio bands (Hada et al. 2012). Note that the M 87 jet has another remarkable feature, called HST-1, located at a deprojected distance of at least 120 pc, although its direct connection with γ-ray activity is still under hot debate (e.g., Chang et al. 2010; Giroletti et al. 2012).

The images in figure 5 show a core and jet feature. Although we fitted only one Gaussian component to the image (figure 2), it is sometimes possible to put an additional component in the jet. However, it highly depends on the *uv*-coverage as to whether we can include this component. Thus, we present model-fit results only for the core (C1).

The flux density of C1 is around 1 Jy, and slightly time variable with a level of 10%–20% during the observing periods presented in this paper (figure 5).

7.4. J1512−0905 (PKS 1510−089)

PKS 1510−089 is an FSRQ at $z = 0.36$ (Thompson et al. 1990). This source was discovered to be a γ-ray source by EGRET and one out of the three FSRQs detected by MAGIC and H.E.S.S. (Wagner 2010; Cortina 2012). Since 2008, the γ-ray emission of PKS 1510−089 became highly variable, and many rapid and intense flaring episodes have been detected by the Italian Space Agency Satellite AGILE and Fermi (e.g., D'Ammando et al. 2009, 2011). In 2011 July and October, two major γ-ray flares were detected. Especially during the latter flare, the source reached the highest γ-ray flux density, becoming the second brightest AGN ever observed by Fermi. Orienti et al. (2012) investigated the connection of historical γ-ray activities with lower energy bands, and GENJI plays an important role in the paper by providing a VLBI core light curve as a part of our first results. The radio-flux density has no apparent correlation with the former γ-ray flare; however, if the latter flare is related to a radio outburst, the correlation indicates that the γ-ray emission region is located ~ 10 pc downstream from the central engine along the jet (Orienti et al. 2012).

We detected radio emission within ~ 3 mas from the core (figures 2d and 6). The radio emission mostly originates in the core (C1), and a faint jet is extending at a position angle of $\sim -30°$. The jet can be represented by a single Gaussian component, C2, in our GENJI image. In the later few epochs, an additional component, C3, can be fitted in the region between C1 and C2 (figure 13). C2 and C3 correspond to N1 and N2 of a higher resolution image by VLBA (figure 4 of Orienti et al. 2011), respectively.

We do not include the flux density of C3 in figure 11d, since C3 appeared to be visible only in the later few epochs. The total flux density decreased from 2.22 Jy on 2010 November 1 to 1.58 Jy on 2010 December 14 (figure 11d). It became bright

Table 3. Summary of Gaussian model parameters of DA 55.

Epoch	Component	Flux [Jy]	Radius [mas]*	θ [°] †	Major [mas]‡	Axial ratio§	ϕ [°]‖
2011/Apr/22	C1	1.803	0.012	115.4	0.212	0.000	−79.4
	C2	0.161	0.971	−49.8	0.606	1.000	−21.8
2011/May/06+May/09	C1	1.820	0.012	123.6	0.107	0.000	71.4
	C2	0.162	0.992	−52.3	0.867	1.000	17.1
2011/May/19	C1	1.877	0.012	123.0	0.291	0.140	−72.0
	C2	0.197	1.050	−48.8	0.726	1.000	0.0

* The radial distance of the component center from the center of the map.
† The position angle of the center of the component.
‡ The FWHM major axis of the component.
§ The ratio of the minor axis to the major axis.
‖ The position angle of the major axis.

Table 4. Summary of Gaussian model parameters of 3C 84.

Epoch	Component	Flux [Jy]	Radius [mas]	θ [°]	Major [mas]	Axial ratio	ϕ [°]
2010/Nov/28	C1	5.980	1.390	−6.3	0.786	0.000	−25.9
	C2	3.506	0.715	−83.2	0.461	1.000	−90.0
	C3	10.112	0.067	125.7	0.688	0.674	−40.6
2010/Nov/29	C1	5.493	1.409	−4.6	0.744	0.451	−20.7
	C2	4.956	0.595	−75.8	0.761	1.000	−101.3
	C3	6.895	0.165	108.9	0.680	0.308	12.7
2010/Nov/29	C1	5.447	1.449	−5.8	0.793	0.423	−19.6
	C2	5.020	0.602	−73.1	0.757	1.000	−90.0
	C3	6.166	0.140	99.3	0.652	0.000	14.7

in 2011 February (2.04 Jy on 2011 February 11 and 2.26 Jy on 2011 February 26), and then subsequently decreased to $\sim$1.5 Jy in 2011 April. The overall trend is similar to the MOJAVE results, but our GENJI light curve provides a more detailed change in the flux density.

7.5. J1613+3412 (DA 406)

DA 406, which is classified as an FSRQ, is the highest-redshift object in the GENJI source list ($z = 1.397$: Schneider et al. 2007). A one-sided jet of the VLBA 15 GHz image extends in a southeasterly direction (Lister et al. 2009). A bright component is located at $\sim$4.5 mas from the core. This source was detected with both EGRET (3EG J1614+3424) and Fermi/LAT (1FGL J1613.5+3411). The γ-ray flux density of this source in EGRET-era was clearly brighter than that in Fermi-era (Piner & Kingham 1997; Abdo et al. 2010d).

Our GENJI images show a bright radio core and a one-sided jet extending at a position angle of $\sim 170°$ (figures 2e and 7). Two components, C1 and C2, can fit with the central $\sim$2 mas structure. Another component, C3, can be fitted to the jet feature at 4.5 mas from the core. No significant motion of these components can be found by the GENJI 7-month monitor.

Our GENJI light curve shows that the flux densities during the later period (from 2011 April 22 to 2011 May 25) clearly increased from those in earlier epochs (figure 11e). MOJAVE provides only a piece of data in these epochs, and therefore this change in the flux density was not detected.

7.6. J1733−1304 (NRAO 530)

NRAO 530 (also known as PKS 1730−13) is a well-known blazar at $z = 0.902$ (Healey et al. 2008), classified as an FSRQ source. NRAO 530 has a strong variability at various wavelengths, such as radio (Bower et al. 1997), optical (Webb et al. 1988), X-ray (Foschini et al. 2006), and γ-ray bands (Mukherjee et al. 1997; D'Ammando & Vandenbroucke 2010). In the γ-ray band, NRAO 530 was identified with the EGRET source 2EG 1735−1312 (Thompson et al. 1995). After the launch of Fermi, it appeared not to be a bright source (Abdo et al. 2009b), but to be a relatively quiescent source, 1FGL J1733.0−1308 (Abdo et al. 2010b). However, its γ-ray activity increased in the latter half of 2010, and NRAO 530 flared during the period from 2010 October 31 to November 2 (D'Ammando & Vandenbroucke 2010). On the parsec-scale, NRAO 530 has a core-jet structure extending northward from the core with a wiggled trajectory on a scale of $\sim$30 mas (Lu et al. 2011).

We detected a structure within 5 mas from the core (figures 2f and 8). The observed structure is consistent with previous VLBI observations. It mainly consists of two major components, C1 and C2, and two faint jet components, C3 and C4 (figure 2).

In figure 11, we show the light curve of the sum of C1 and C2, since the distance between C1 and C2 is very small, and the flux density of C1 can be correlated with that of C2. In some epochs, we could not distinguish C2 from C1, or we

Table 5. Summary of Gaussian model parameters of M 87.

Epoch	Component	Flux [Jy]	Radius [mas]	θ [°]	Major [mas]	Axial ratio	ϕ [°]
2010/Nov/04	C1	1.131	0.046	−77.3	0.796	0.384	−60.8
2010/Dec/04	C1	1.120	0.035	−85.0	0.695	0.515	−59.5
2010/Dec/16	C1	1.205	0.031	−73.9	0.716	0.694	−52.0

Table 6. Summary of Gaussian model parameters of PKS 1510−089.

Epoch	Component	Flux [Jy]	Radius [mas]	θ [°]	Major [mas]	Axial ratio	ϕ [°]
2010/Nov/18	C1	1.968	0.008	−88.2	0.538	0.349	−33.6
	C2	0.129	2.523	−30.8	1.614	0.292	−17.3
2010/Nov/29	C1	1.817	0.014	−47.1	0.618	0.368	−30.7
	C2	0.112	2.474	−36.1	0.777	0.546	−25.6
2010/Dec/04	C1	1.771	0.022	−50.7	0.544	0.436	−30.4
	C2	0.081	2.118	−33.6	0.000	1.000	0.0

Table 7. Summary of Gaussian model parameters of DA 406.

Epoch	Component	Flux [Jy]	Radius [mas]	θ [°]	Major [mas]	Axial ratio	ϕ [°]
2010/Dec/21	C1	1.256	0.007	7.647	1.491e-08	1.000	−3.5
	C2	0.110	4.355	157.1	0.826	1.000	8.5
	C3	0.041	1.043	170.5	0.607	1.000	−12.2
2011/Jan/09+Jan/15	C1	1.113	0.034	−2.8	1.761e-07	1.000	−8.5
	C2	0.049	4.303	158.8	0.194	1.000	0.0
	C3	0.149	0.526	177.7	0.533	1.000	−8.5
2011/Feb/02	C1	1.281	0.012	−2.1	0.130	1.000	−36.2
	C2	0.056	4.202	160.1	0.660	1.000	−10.1
	C3	0.071	0.798	168.8	5.067e-07	1.000	−5.6

Table 8. Summary of Gaussian model parameters of NRAO 530.

Epoch	Component	Flux [Jy]	Radius [mas]	θ [°]	Major [mas]	Axial ratio	ϕ [°]
2010/Nov/11	C1	2.733	0.118	−170.1	0.000	1.000	0.0
	C2	1.405	0.254	6.6	0.000	1.000	0.0
	C3	0.118	2.682	−3.9	1.723	0.000	−36.2
2010/Nov/14	C1	2.594	0.129	−177.1	0.000	1.000	0.0
	C2	1.573	0.228	2.7	0.000	1.000	0.0
	C3	0.174	2.715	−3.8	1.517	0.516	−30.886
2010/Nov/16	C1	2.925	0.092	−168.0	0.000	1.000	0.0
	C2	1.142	0.262	11.9	0.000	1.000	0.0
	C3	0.130	2.639	−6.1	1.869	0.456	−46.8

could not detect C3 and C4, presumably due to lack of *uv*-coverage. We do not include the light curve of C4 in figure 11, since the fit is not quite robust. Our observations started 9 days after the 2010 October γ-ray flare. Our results show that the core-flux density of NRAO 530 increased from ~ 2.7 Jy to ~ 4.0 Jy at the end of 2010. The flux density of the flared core was relatively stable until 2011 May, and then started to decrease in 2011 May. It is difficult to follow the change in the flux density during this period only with MOJAVE. NRAO 530 is one of the most successful examples in showing us how important for studying the connection between a γ-ray flare and the change in the radio-flux density the intensive monitoring provided by GENJI is.

7.7. J2202+4216 (BL Lac)

BL Lac ($z = 0.0686$: Sazonov et al. 2007) is a prototypical blazar that has been well studied across the entire electromagnetic spectrum. This source has been detected by EGRET several times, and is now routinely detected by Fermi (Abdo et al. 2011). Above 200 GeV, significant detection was made by

Table 9. Summary of Gaussian model parameters of BL Lac.

Epoch	Component	Flux [Jy]	Radius [mas]	θ [°]	Major [mas]	Axial ratio	ϕ [°]
2011/Feb/08	C1	2.477	0.054	171.7	0.598	0.000	41.5
	C2	0.593	2.125	−165.5	0.788	0.743	−6.9
2011/Feb/12	C1	2.175	0.006	171.6	0.330	0.000	45.4
	C2	0.843	2.038	−167.8	2.137	0.306	10.3
2011/Feb/13	C1	2.489	0.015	158.1	0.423	0.333	20.0
	C2	0.680	1.945	−169.0	1.265	0.445	17.2

Table 10. Summary of Gaussian model parameters of 3C 454.3.

Epoch	Component	Flux [Jy]	Radius [mas]	θ [°]	Major [mas]	Axial ratio	ϕ [°]
2010/Nov/10	C1	21.039	0.053	79.1	0	1	0
	C2	3.987	0.363	−102.7	0	1	0
2010/Nov/12	C1	21.230	0.041	80.9	0	1	0
	C2	2.771	0.423	−100.2	0	1	0
2010/Dec/11	C1	21.487	0.046	76.0	0	1	0
	C2	3.456	0.390	−104.3	0	1	0

MAGIC (Albert et al. 2007). The VLBI structure of this source is characterized by the bright core and the jet propagating southward (e.g., Jorstad et al. 2005; Bach et al. 2006). A recent multiwavelength study detected a multiple γ-ray flaring event that is followed by the emergence of a superluminal knot from the core, together with a continuous rotation of the optical polarization angle (Marscher et al. 2008). These lead to the scenario that the flaring event in this source is produced downstream at a large distance (more than 1 pc or 10^4 R_s) of the central engine, although such an interpretation is still controversial (Tavecchio et al. 2010).

We detected the bright core (C1) and a jet feature extending to a few mas from the core. The jet feature can be represented as a single Gaussian component, C2 (figure 2g).

The difference in the flux density between our GENJI light curve and MOJAVE (see figure 11g) can be explained by the contribution from the extended jet, since a continuous jet extending up to more than 5 mas from the core is seen on the MOJAVE images (Lister et al. 2009). The flux density decreased from 4.0 Jy on 2010 November 22 to 2.5 Jy on 2011 January 15, and then a small rise and decay in the flux density was seen about two months between 2011 February and March. In later epochs, the flux density increased slightly from 2.6 Jy on 2011 March 2 to 3.2 Jy on 2011 May 22.

7.8. 3C 454.3

A well-known FSRQ source, 3C 454.3, at $z = 0.859$ (Sazonov et al. 2007) is one of the brightest extragalactic radio sources. After 2000, the radio-flux density of 3C 454.3 has been quite time variable, and showed increased activity time after time. In particular since 2005, a remarkable flaring activity has been seen in this source over the whole electromagnetic spectrum ranging from radio to γ-rays. During the last four years, this source has exhibited more than one γ-ray flare every year, becoming the most active γ-ray blazar in the sky. The largest flare occurred in 2010 November. In this flare, 3C 454.3 reached a peak flux density that is more than six times the flux density of the brightest steady γ-ray source, the Vela pulsar, and more than three times its previous superflare on 2009 December 2–3 (Abdo et al. 2011; Vercellone et al. 2011). On the parsec-scale, 3C 454.3 has a core-jet structure extending westward. Previous VLBI observations showed jet components propagating along different trajectories (Lister et al. 2009).

We detected a structure within 1 mas from the core. It mainly consists of two major components, C1 and C2 (figure 2h).

In figure 10, we show the sum of the flux densities of C1 and C2, since the distance between C1 and C2 is very small and the flux density of C1 can be correlated with that of C3. Our observations started just before the largest γ-ray flare in 2010 November. Our results show that the core flux of 3C 454.3 started to increase in 2010 December, and peaked at around 2011 February. This is consistent with the idea that the γ-ray flaring region is located at the upstream side of the radio core, and that the increase in the flux density of the radio core is the result of the propagation of the flaring component. If we assume a jet speed of $\Gamma = 10$ (Γ is the bulk Lorentz factor), the γ-ray flaring zone should be located at an ~ 0.05 pc upstream side of the 22 GHz radio core. We note that the rise and decay of the flux density are visible from the GENJI light curve, but are not very apparent from the MOJAVE light curve (figure 11).

8. Summary

We have presented the first 7-month results from the GENJI programme. In this paper, we particularly focused on the fidelity of the image and the flux-density measurement by comparing nearby epoch data. We also presented the consistency with MOJAVE. We will discuss the details of light curve and the kinematics for individual sources in separate papers. In particular, we successfully obtained data just before/after the γ-ray flares reported in PKS 1510−089, NRAO 530,

and 3C 454.3. The 22 GHz data from GENJI are unique, and provide complementary information to other monitoring projects in radio bands.

We thank the anonymous referee for helpful comments. We are grateful to the staff of all VERA stations for their assistance in observations. This research has made use of the NASA/IPAC Extragalactic Database (NED), which is operated by the Jet Propulsion Laboratory, California Institute of Technology, under contract with the National Aeronautics and Space Administration. This research has made use of data from the MOJAVE database, which is maintained by the MOJAVE team (Lister et al. 2009). The VLBA is operated by the US National Radio Astronomy Observatory (NRAO), a facility of the National Science Foundation operated under a cooperative agreement by Associated Universities, Inc. Part of this work was done with contributions by the Italian Ministry of Foreign Affairs and University and Research for collaboration projects between Italy and Japan. This work is partially supported by a Grant-in-Aid for Scientific Research, KAKENHI 24540240 (MK) from Japan Society for the Promotion of Science (JSPS).

References

Abdo, A. A., et al. 2009a, ApJ, 699, 31
Abdo, A. A., et al. 2009b, ApJ, 700, 597
Abdo, A. A., et al. 2009c, ApJ, 707, 55
Abdo, A. A., et al. 2010a, ApJ, 720, 912
Abdo, A. A., et al. 2010b, Nature, 463, 919
Abdo, A. A., et al. 2010c, ApJ, 722, 520
Abdo, A. A., et al. 2010d, ApJS, 188, 405
Abdo, A. A., et al. 2011, ApJ, 733, L26
Abramowski, A., et al. 2012, ApJ, 746, 151
Acciari, V. A., et al. 2009, Science, 325, 444
Aharonian, F., et al. 2006, Science, 314, 1424
Albert, J., et al. 2007, ApJ, 666, L17
Aleksić, J., et al. 2012, A&A, 539, L2
Asada, K., Kameno, S., Shen, Z.-Q., Horiuchi, S., Gabuzda, D. C., & Inoue, M. 2006, PASJ, 58, 261
Bach, U., et al. 2006, A&A, 456, 105
Bower, G. C., Backer, D. C., Wright, M., Forster, J. R., Aller, H. D., & Aller, M. F. 1997, ApJ, 484, 118
Brown, A. M., & Adams, J. 2011, MNRAS, 413, 2785
Chang, C. S., Ros, E., Kovalev, Y. Y., & Lister, M. L. 2010, A&A, 515, A38
Chikada, Y., Kawaguchi, N., Inoue, M., Morimoto, M., Kobayashi, H., & Mattori, S. 1991, in Frontiers of VLBI, ed. H. Hirabayashi et al. (Tokyo: Universal Academy Press), 79
Cortina, J. 2012, Astron. Telegram, 4583
D'Ammando, F., et al. 2009, A&A, 508, 181
D'Ammando, F., et al. 2011, A&A, 529, A145
D'Ammando, F., & Vandenbroucke, J. 2010, Astron. Telegram, 3002
Foschini, L., et al. 2006, A&A, 450, 77
Gebhardt, K., & Thomas, J. 2009, ApJ, 700, 1690
Giroletti, M., et al. 2012, A&A, 538, L10
Hada, K., et al. 2012, ApJ, 760, 52
Hada, K., Doi, A., Kino, M., Nagai, H., Hagiwara, Y., & Kawaguchi, N. 2011, Nature, 477, 185
Healey, S. E., et al. 2008, ApJS, 175, 97
Iguchi, S., Kurayama, T., Kawaguchi, N., & Kawakami, K. 2005, PASJ, 57, 259
Jorstad, S. G., et al. 2005, AJ, 130, 1418
Kataoka, J., et al. 2010, ApJ, 715, 554
Kellermann, K. I., Vermeulen, R. C., Zensus, J. A., & Cohen, M. H. 1998, AJ, 115, 1295
Komatsu, E., et al. 2011, ApJS, 192, 18
Kubo, H., Takahashi, T., Madejski, G., Tashiro, M., Makino, F., Inoue, S., & Takahara, F. 1998, ApJ, 504, 693
Lister, M. L., et al. 2009, AJ, 138, 1874
Lister, M. L., et al. 2011, ApJ, 742, 27
Lu, R.-S., Krichbaum, T. P., & Zensus, J. A. 2011, MNRAS, 418, 2260
Marscher, A. P., et al. 2008, Nature, 452, 966
Marscher, A. P., et al. 2010, ApJ, 710, L126
Mukherjee, R., et al. 1997, ApJ, 490, 116
Nagai, H., et al. 2010, PASJ, 62, L11
Nagai, H., et al. 2012, MNRAS, 423, L122
Nolan, P. L., et al. 2012, ApJS, 199, 31
O'Dea, C. P., Dent, W. A., & Balonek, T. J. 1984, ApJ, 278, 89
Ojha, R., et al. 2010, A&A, 519, A45
Orienti, M., et al. 2012, A&A submitted
Orienti, M., Venturi, T., Dallacasa, D., D'Ammando, F., Giroletti, M., Giovannini, G., Vercellone, S., & Tavani, M. 2011, MNRAS, 417, 359
Petrosian, A., McLean, B., Allen, R. J., & MacKenty, J. W. 2007, ApJS, 170, 33
Petrov, L., Honma, M., & Shibata, S. M. 2012, AJ, 143, 35
Piner, B. G., & Kingham, K. A. 1997, ApJ, 479, 684
Rines, K., & Geller, M. J. 2008, AJ, 135, 1837
Sazonov, S., Revnivtsev, M., Krivonos, R., Churazov, E., & Sunyaev, R. 2007, A&A, 462, 57
Schneider, D. P., et al. 2007, AJ, 134, 102
Sikora, M., Stawarz, Ł., Moderski, R., Nalewajko, K., & Madejski, G. M. 2009, ApJ, 704, 38
Sokolovsky, K. V., Kovalev, Y. Y., Lobanov, A. P., Savolainen, T., Pushkarev, A. B., & Kadler, M. 2010, in Proc. 2009 Fermi Symp., eConf C0911022, arXiv:1001.2591
Suzuki, K., et al. 2012, ApJ, 746, 140
Tavecchio, F., Ghisellini, G., Ghirlanda, G., Foschini, L., & Maraschi, L. 2010, MNRAS, 401, 1570
Thompson, D. J., et al. 1995, ApJS, 101, 259
Thompson, D. J., Djorgovski, S., & de Carvalho, R. 1990, PASP, 102, 1235
Vercellone, S., et al. 2011, ApJ, 736, L38
Wagner, S. 2010, Abstract, Am. Astron. Soc., 11th Div. Meeting, 27.06
Walker, R. C., Dhawan, V., Romney, J. D., Kellermann, K. I., & Vermeulen, R. C. 2000, ApJ, 530, 233
Webb, J. R., Smith, A. G., Leacock, R. J., Fitzgibbons, G. L., Gombola, P. P., & Shepherd, D. W. 1988, AJ, 95, 374